JMR Journal of Meteorological Research

ENSO–Like Pacing of the Asian Summer Monsoon during the Early Holocene

Xiaohua SHAO, Tao WANG, Yongjin WANG, Hai CHENG, Kan ZHAO, Xinggong KONG

Citation: Xiaohua SHAO, Tao WANG, Yongjin WANG, Hai CHENG, Kan ZHAO, Xinggong KONG, 2020. ENSO–Like Pacing of the Asian Summer Monsoon during the Early Holocene, Journal of Meteorological Research, 34, 325–335. doi: 10.1007/s13351–020–9079–9.

View online: https://doi.org/10.1007/s13351–020–9079–9

ENSO-Like Pacing of the Asian Summer Monsoon during the Early Holocene

Xiaohua SHAO[1*], Tao WANG[2], Yongjin WANG[3,4], Hai CHENG[5,6], Kan ZHAO[3,4], and Xinggong KONG[3,4]

1 *School of Geography, Nanjing University of Information Science & Technology, Nanjing* 210044, *China*
2 *Public Meteorological Service Center of Anhui Province, Hefei* 230031, *China*
3 *Key Laboratory of Virtual Geographic Environment, Ministry of Education, Nanjing Normal University, Nanjing* 210023, *China*
4 *Jiangsu Center for Collaborative Innovation in Geographical Information Resource Development and Application, Nanjing* 210023, *China*
5 *Institute of Global Environmental Change, Xi'an Jiaotong University, Xi'an* 710049, *China*
6 *Department of Geology and Geophysics, University of Minnesota, MN* 55455, *USA*

(Received May 30, 2019; in final form November 19, 2019)

ABSTRACT

We present a ^{230}Th-dated stalagmite oxygen isotope (δ^{18}O) record from Loushanguan Cave in the Yangtze River valley, China. The δ^{18}O record, if viewed as a proxy of the Asian summer monsoon (ASM) intensity, provides an ASM history for the early Holocene with clear centennial-scale variability. A significant approximately 200-yr cycle between 10.2 and 9.1 ka BP (before present, where "present" is defined as the year AD 1950), as revealed by spectral power analyses, is of global significance and is probably forced by the Suess or de Vries cycle of solar activity. Here, we explore a physical mechanism to explain the relationship between the solar activity and the ASM. A strong coherence between the ASM and El Niño–Southern Oscillation (ENSO) has been observed by performing cross-wavelet analyses on this cycle. Our study suggests that a strong (weak) ASM state corresponds to a warm (cold) ENSO, which is consistent with modern meteorological observations but contrasts with previous studies on regions far from the Meiyu rainbelt. We argue that the centennial fluctuations of the ASM are a fundamental characteristic forced by the solar activity, with the ENSO variability as a mediator. The relationship between ENSO and the ASM displayed spatial heterogeneity on the centennial scale during the early Holocene, which is a more direct analogue to the observed modern interannual variability of the ASM.

Key words: isotope records, Asian summer monsoon, El Niño–Southern Oscillation, centennial scale, solar activity, Yangtze River valley, early Holocene

Citation: Shao, X. H., T. Wang, Y. J. Wang, et al., 2020: ENSO-like pacing of the Asian summer monsoon during the early Holocene. *J. Meteor. Res.*, **34**(2), 325–335, doi: 10.1007/s13351-020-9079-9.

1. Introduction

El Niño–Southern Oscillation (ENSO) is earth's dominant source of interannual climate variability (Collins et al., 2010). Numerous observational studies have suggested that the all-Indian rainfall, which represents the strength of the Indian summer monsoon (ISM) circulation (Parthasarathy et al., 1994; Pai, 2004), is negatively correlated with ENSO indices (weak monsoons arising from warm ENSO events) on interannual to decadal timescales (e.g., Rasmusson and Carpenter, 1983; Ropelewski and Halpert, 1987; Webster and Yang, 1992). In agreement with the observed results, numerical simulations suggest that years with warm sea surface temperature (SST) anomalies in the equatorial central and East Pacific Ocean (El Niño) have weaker ISM circulations and delayed onsets of the ISM (e.g., Ju and Slingo, 1995). This relationship between the ISM and ENSO may have been weakened or broken down over recent decades (e.g., Kumar et al., 1999; Kinter et al., 2002).

The East Asian summer monsoon (EASM), which is another major component of the Asian summer monsoon (ASM), has complex spatial and temporal structures that are distinct from the ISM (Chang et al., 2000; Wang et al., 2008). The SST anomalies of the tropical ocean (e.g.,

Supported by the National Natural Science Foundation of China (40701013, 41877453, and 41572151) and National Key Research and Development Program of China (2018YFA0605603).

*Corresponding author: xiaohua.shao@nuist.edu.cn.

the western Pacific warm pool), which have been identified as influential to the EASM (e.g., Huang and Lu, 1989; Shen and Lau, 1995; Nitta and Hu, 1996), are to a certain degree all related to ENSO (Wang et al., 2000). However, it has not been possible to find significant correlations between the eastern Pacific SST anomalies and the EASM circulation or precipitation on the interannual timescale (e.g., Chen et al., 1992; Wang, 2002; Wang et al., 2008). The relationship between the EASM and ENSO is unstable and exhibits considerable interdecadal differences (e.g., Wang et al., 2008, 2009; Li et al., 2010; Wu et al., 2012). It is interesting that there has been a strengthening of the ENSO–EASM relationship within the past 50 years, which is opposite to the situation for the ISM (Wang et al., 2008; Li et al., 2010).

The relationships between the ASM and ENSO determined from modern observations are chaotic. They may be very different from those under basic climate states owing to the current situation in terms of global warming (Kumar et al., 1999; Li et al., 2010). How and why the correlations between the ASM and ENSO change on longer than interannual to decadal timescales is therefore of broad interest. Quite a few paleoclimate studies, based mainly on tree rings, stalagmites, simulations, etc., have suggested that a warm ENSO is always related to a weak ASM or a drought in the ASM region, on multiple timescales (e.g., Kumar et al., 2006; Cook et al., 2010; Marchitto et al., 2010; Zhao et al., 2016). However, less attention has been paid to the relationship between the ASM and ENSO on the centennial scale during the early Holocene. The early Holocene warming coincided with a period when the ice-free land areas in polar areas at the time were being rapidly uncovered by the melting ice sheet (Corbett et al., 2011; Larsen et al., 2011; Hughes et al., 2012). The possible absence of ENSO variability during the early Holocene is still controversial (e.g., Moy et al., 2002; Rodó and Rodriguez-Arias, 2004; Carré et al., 2014; Chen et al., 2016). Unraveling the relationship between the ASM and ENSO on the centennial scale during the early Holocene is, therefore, essential both to understanding the central role of the tropical oceans in the regulation of monsoon climate on the centennial scale, and to effectively predicting future monsoon climate changes under the projected global warming scenarios.

Here, we present an ASM record of the early Holocene with an approximately 11-yr resolution and clear centennial-scale fluctuations between 10.2 and 9.1 ka BP (before present, where "present" is defined as the year AD 1950) from Loushanguan Cave, China. This record allows us to do the following: (1) detect the centennial-scale ASM variability during the early Holocene associated with the ENSO signal and (2) investigate the relationship between ENSO and ASM variabilities on the centennial scale. This should provide new insights into the debated issue (Lau and Weng, 2001) on the phasing of the ASM and ENSO, which is plausibly forced by solar activity.

2. Materials and methods

2.1 *Study site and sampling*

Loushanguan Cave (28°12′N, 106°51′E; elevation: 1115 m) is located in the Yangtze River valley, China (Fig. 1). The cave is about 80 m long. In East Asia, a subtropical front is most prominent during June and July, which stretches for many thousands of kilometers, producing an almost east–west-elongated rainbelt (e.g., Ding, 2004; Ninomiya, 2004; Wang et al., 2008). The intense rains during that period are called Meiyu in China, Baiu in Japan, and Changma in Korea (Wang et al., 2008). The mean maximum rainfall during the mature monsoon (Meiyu) occurs in the Yangtze River valley (Chang et al., 2000). The annual mean temperature and multi-year average of annual rainfall in this area are approximately 15.1°C and 1100 mm, respectively. The area is strongly affected by the ASM system. About 80% of total annual precipitation falls during the monsoon months (May–October), when convective monsoon rainfall prevails (1971–2000 AD, from a local meteorological station). The oxygen isotope ratios (reported relative to the Vienna Standard Mean Ocean Water) from the rainwater collected in Zunyi (27°42′N, 106°53′E; elevation: 844 m; 35 km south of Loushanguan Cave) range between −3.24‰ in the winter (December–February) and −9.92‰ in the summer (June–August), with an annual average of −6.57‰ (1986–1991 AD, from the Global Network of Isotopes in Precipitation database, https://nucleus.iaea.org/wiser).

Stalagmite LSG (21 cm long; Fig. 2) was collected approximately 10 m from the cave entrance in 2010. The sample was halved along its growth axis and then polished. The polished surface of the stalagmite displays complex brown–yellow color variations with bands up to a few millimeters wide (Fig. 2).

2.2 *Analytic methods*

Eleven sub-samples were collected for ^{230}Th dating.

The procedures for chemical separation and purification of uranium and thorium are similar to those described in Cheng et al. (2000). ^{230}Th dating was performed in two labs [(1) the Isotope Laboratory at the University of Minnesota, USA and (2) the Isotope Laboratory of Nanjing Normal University in Nanjing, China] using a multi-collector inductively coupled plasma mass spectrometer (MC-ICP-MS, Thermo-Finnigan Neptune). A total of

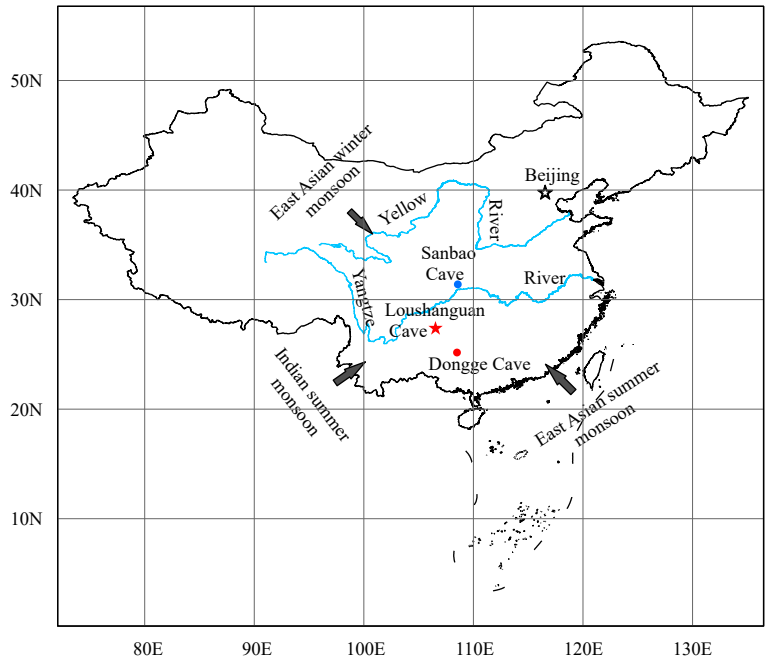

Fig. 1. Sketch map showing the location of Loushanguan Cave (red star; this study). Sanbao Cave (blue dot; Dong et al., 2010) and Dongge Cave (red dot; Dykoski et al., 2005; Wang et al., 2005) are also included. The arrows depict the East Asian summer and winter monsoons and the Indian summer monsoon.

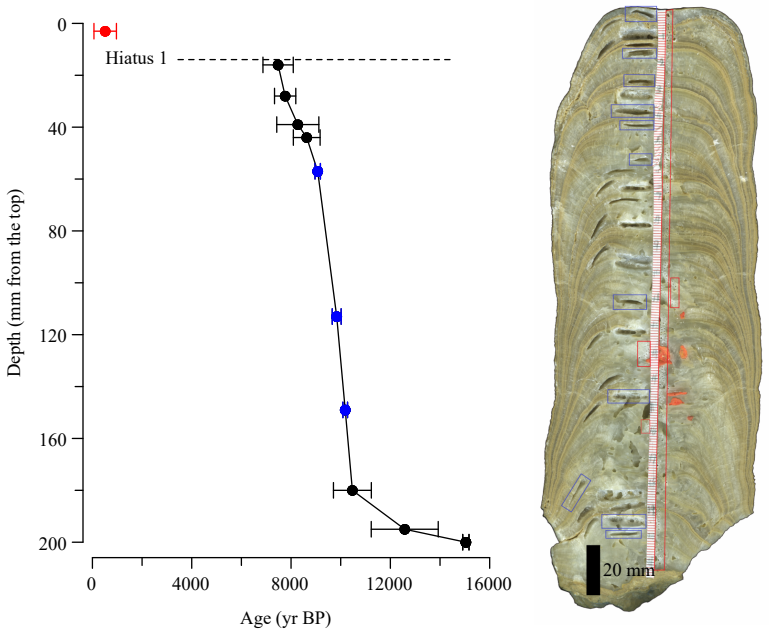

Fig. 2. Left: Age–depth relation for the LSG sample. The chronology is established using linear interpolation. The ages are specified in years BP (before the year AD 1950). The horizontal error bars depict the errors of the ^{230}Th dates. The ^{230}Th ages used to construct the age model are shown in blue and black, and the excluded age is in red. The blue dots indicate the three high-precision dates with relative analytical errors between ± 0.9% and ± 1.8%. The hiatus is indicated by the dashed black line. Right: Scan of cut and polished stalagmite LSG with the sampling locations for the isotopic analysis (dots in red boxes) and dating (blue boxes). Black bar marked as 20 mm is an indicator of the scale.

210 sub-samples were taken with a 0.3-mm diameter hand-held carbide dental drill at a spacing of 1 mm for stable oxygen and carbon isotope analysis. The analyses were performed in the Isotope Laboratory of Nanjing Normal University with a mass spectrometer (MAT-253). The precision of the $\delta^{18}O$ values was 0.06‰ at the 1σ level.

3. Results

3.1 *Chronology*

Stalagmite LSG grew between 15.0 and 0.5 ka BP, with an obvious hiatus at around 7.5–0.5 ka BP (Table 1). This hiatus was identified in the depth–age relationship, coinciding with the dark brown layer in the stalagmite (Fig. 2). Ten ^{230}Th dates, with relative analytical errors between ± 0.9% and ± 10.7%, were identified to develop the age model (Table 1, Fig. 2). Linear interpolation was used to calculate the age for each $\delta^{18}O$ value. Therefore, comparisons with other ASM records during the early Holocene are restricted to the long-term trend in the LSG oxygen isotope data. The sampling interval between 10.2 and 9.1 ka BP of stalagmite LSG yielded an average temporal resolution of approximately 11 yr. In addition, the age model of this interval was based on three high-precision dates with relative analytical errors between ± 0.9% and ± 1.8% (shown in blue in Fig. 2). Therefore, we can tentatively compare the LSG records of this interval with other available records on the centennial scale, since this kind of age model is sufficient to resolve this temporal variability.

3.2 *The $\delta^{18}O$ record*

Stalagmite LSG's $\delta^{18}O$ profiles vary from −9.1‰ to −11.1‰ (blue dots and line in Fig. 3), with an average value of −10.3‰. At the onset of the Holocene, the $\delta^{18}O$ values are very heavy, and then they decrease abruptly from −9.1‰ to −10.1‰. After that jump, the $\delta^{18}O$ becomes persistently lighter until its values reach a peak at approximately 9.5 ka, before then remaining steady for several thousand years with only minor fluctuations and an average value of −10.4‰. This general pattern is interrupted by several positive excursions that are centered at approximately 7.8, 8.7, 9.1, 9.5, 9.7, and 10 ka BP (shown as bars in Fig. 3), each with an amplitude of approximately 1‰. According to the chronology, four of the six events, which are centered at approximately 9.1, 9.5, 9.7, and 10 ka BP (shown as pink bars in Fig. 3), are more reliable.

Table 1. ^{230}Th dating results for stalagmite LSG

Sample number	Depth (mm from the top)	^{238}U (ppb)	^{232}Th (ppt)	^{230}Th / ^{232}Th (atomic × 10^{-6})	$\delta^{234}U$* (measured)	^{230}Th / ^{238}U (activity)	^{230}Th age (yr) (uncorrected)	$\delta^{234}U_{initial}$** (corrected)	^{230}Th age (yr BP)*** (corrected)
LSG-3	3	136.00 ± 0.13	12138.19 ± 12.05	1.26 ± 0.01	1817.07 ± 1.39	0.0370 ± 0.0003	1440 ± 12	1819.71 ± 1.39	515 ± 453
LSG-16	16	109.82 ± 0.06	13068.29 ± 15.91	5.60 ± 0.02	1812.13 ± 1.28	0.2171 ± 0.0009	8689 ± 39	1850.79 ± 1.30	7479 ± 610
LSG-28	28	139.16 ± 0.09	11531.50 ± 13.87	7.97 ± 0.03	1823.89 ± 1.17	0.2160 ± 0.0008	8605 ± 31	1864.29 ± 1.19	7763 ± 428
LSG-39	39	133.34 ± 0.09	21938.93 ± 27.24	4.61 ± 0.02	1825.02 ± 1.21	0.2487 ± 0.0010	9953 ± 41	1868.13 ± 1.23	8272 ± 847
LSG-44	44	95.65 ± 0.06	10309.60 ± 12.12	6.98 ± 0.02	1867.55 ± 1.30	0.2464 ± 0.0009	9706 ± 38	1913.60 ± 1.33	8632 ± 539
LSG-57	57	104.20 ± 0.03	1978.64 ± 4.04	37.93 ± 0.22	1886.43 ± 1.10	0.2371 ± 0.0014	9263 ± 55	1935.36 ± 1.13	9073 ± 109
LSG-113	113	143.60 ± 0.05	4821.98 ± 9.68	23.20 ± 0.10	1846.71 ± 1.91	0.2561 ± 0.0011	10179 ± 48	1898.71 ± 1.97	9839 ± 179
LSG-149	149	199.47 ± 0.05	2776.53 ± 5.41	57.23 ± 0.27	1862.33 ± 1.12	0.2609 ± 0.0015	10321 ± 63	1916.62 ± 1.15	10182 ± 93
LSG-180	180	157.05 ± 0.10	23592.83 ± 23.76	6.10 ± 0.02	1845.54 ± 1.19	0.2997 ± 0.0009	11998 ± 39	1900.88 ± 1.23	10471 ± 763
LSG-195	195	65.50 ± 0.10	12462.00 ± 250.00	31.00 ± 1.00	1862.10 ± 4.50	0.3621 ± 0.0009	14543 ± 45	1930.00 ± 9.00	12579 ± 1349
LSG-200	200	139.94 ± 0.06	3213.62 ± 6.78	50.41 ± 0.19	1862.83 ± 1.26	0.3793 ± 0.0013	15269 ± 55	1943.60 ± 1.32	15041 ± 126

Note: (1) Errors are 2σ analytical errors. (2) U decay constants: $\lambda_{238} = 1.55125 \times 10^{-10}$ yr^{-1} (Jaffey et al., 1971) and $\lambda_{234} = 2.82206 \times 10^{-6}$ yr^{-1} (Cheng et al., 2013). Th decay constant: $\lambda_{230} = 9.1705 \times 10^{-6}$ yr^{-1} (Cheng et al., 2013). (3) *$\delta^{234}U = ([^{234}U/^{238}U]_{activity} - 1) \times 1000$. **$\delta^{234}U_{initial}$ was calculated based on ^{230}Th age (T), i.e., $\delta^{234}U_{initial} = \delta^{234}U_{measured} \times e^{\lambda_{234} \times T}$. (4) Corrected ^{230}Th ages assume the initial $^{230}Th/^{232}Th$ atomic ratio of $(4.4 \pm 2.2) \times 10^{-6}$. Those are the values for a material at secular equilibrium, with the bulk earth $^{232}Th/^{238}U$ value of 3.8. The errors are arbitrarily assumed to be 50%.

***BP stands for "before present," where "present" is defined as the year AD 1950.

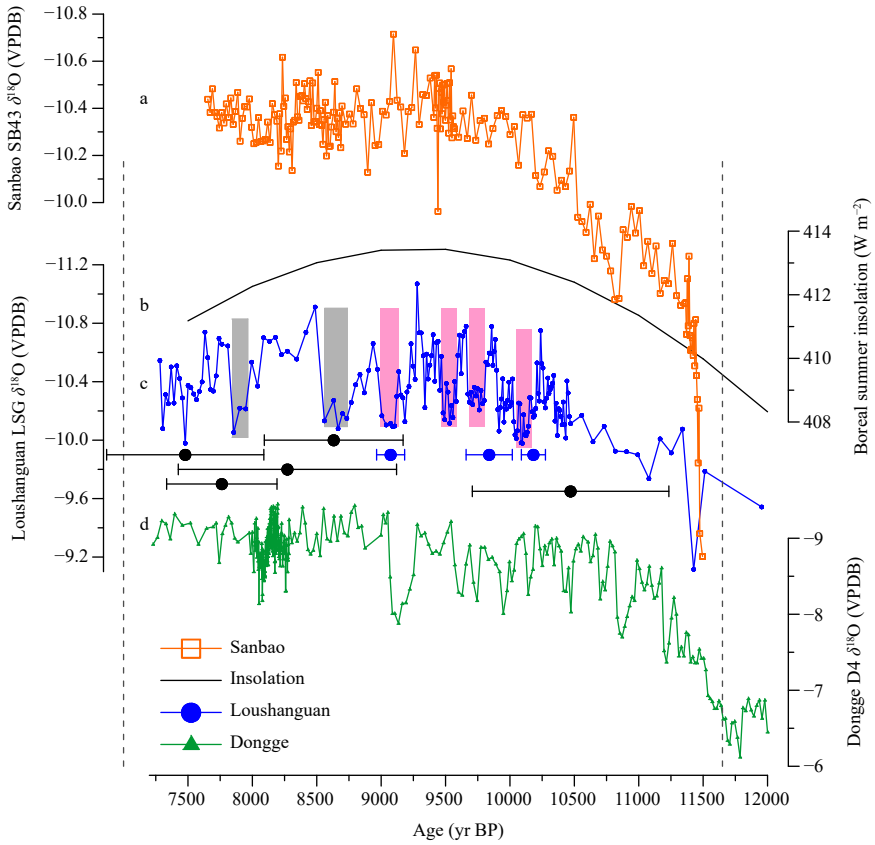

Fig. 3. Comparison of the LSG record with other stalagmite $\delta^{18}O$ records and the boreal summer insolation: (a) the Sanbao Cave record (SB43, orange; Dong et al., 2010), (b) the boreal summer insolation (black; Berger, 1978), (c) the $\delta^{18}O$ record of LSG (blue; this study), and (d) the Dongge Cave record (D4, green; Dykoski et al., 2005). The vertical grey and pink bars indicate six positive excursions of LSG $\delta^{18}O$ values. The blue and black horizontal error bars under the LSG record depict the errors of the ^{230}Th dates. The two vertical dashed grey lines represent the early Holocene time range (ca. 11,650–7000 yr BP) according to Smith et al. (2011).

4. Discussion

4.1 *Regional correlation with other records*

Replication is a rigorous test for isotopic equilibriums (Dorale and Liu, 2009). However, due to dating errors, comparative discussion with other ASM records is restricted to the long-term trend during the early Holocene and to the centennial-scale fluctuations between 10.2 and 9.1 ka BP. Similar to other stalagmite records from the ASM region (Dykoski et al., 2005; Dong et al., 2010), the $\delta^{18}O$ values in stalagmite LSG (Fig. 3c) are high before the onset of the Holocene, and then abruptly fall to lower values, before finally remaining at low values after 10.5 ka BP (Fig. 3).

Today's ASM rainfall is anomalously low in terms of $\delta^{18}O$, meaning that a higher proportion of regional ASM rainfall in annual totals would result in more negative stalagmite $\delta^{18}O$ (e.g., Wang et al., 2005; Cheng et al., 2009; Dong et al., 2010). The stalagmite $\delta^{18}O$ record can be viewed as a measure of the amount of summer monsoon precipitation or "summer monsoon intensity" (Cheng et al., 2009). Therefore, the changes in stalagmite LSG's $\delta^{18}O$ record, which are generally consistent with the shifts in the Dongge and Sanbao records, broadly imply variations of the large-scale summer monsoon strength across the whole southern Asian region. The LSG $\delta^{18}O$ values decrease as the ASM intensifies, and vice versa. The LSG $\delta^{18}O$ time series shows that the ASM intensity was significantly enhanced from the late glacial period to the early Holocene, broadly following the boreal summer insolation. Correlation between the monsoon intensity and insolation during the early Holocene has been demonstrated by other records of the ASM (Dykoski et al., 2005; Dong et al., 2010; Liu et al., 2015; Wu et al., 2018). It indicates that the broad trend of the ASM during this interval is caused by insolation change.

Similar long-term trends and millennial oscillations (e.g., 8.2-, 9.4-, and 10.3-ka events) have been reconstructed from several stalagmite records of the ASM during the early Holocene (Dykoski et al., 2005; Dong et al., 2010; Cai et al., 2012; Liu et al., 2015; Huang et al.,

2016). However, due to the uncertainties in the dating and the different temporal resolutions of ASM records, the timing and structure of centennial fluctuations are not precisely correlated with each other during the early Holocene. Among the three cave records in Fig. 3, the centennial-scale δ^{18}O variations are exceptionally clear in our record between 10.2 and 9.1 ka BP, with a magnitude of approximately 1‰ (Fig. 3). The well-dated (errors: about 1%, Table 1) and high-resolution (about 11 yr) LSG δ^{18}O record between 10.2 and 9.1 ka BP allows us to examine the centennial-scale fluctuations of the ASM during this interval. Spectral analyses of the LSG δ^{18}O data reveal a centennial cycle of about 200 yr with a confidence level greater than 90% (Fig. 4). Similarly, approximately 200-yr climatic variations have also been detected in climate-linked processes in Asia (Burns et al., 2002; Fleitmann et al., 2003; Wang et al., 2005; Raspopov et al., 2008; Liu et al., 2015; Zhao et al., 2015), Europe (Muñoz et al., 2015), North and South America (Peterson et al., 1991; Anderson, 1992; Springer et al., 2008), Australia (Cook et al., 1996), and Antarctica (Zhao and Feng, 2015). This may indicate that the approximately 200-yr cycle is globally significant. The approximately 200-yr cycle, which is called the Suess or de Vries cycle, has been identified as one of the two distinctive quasi-periodic components of Holocene solar activity (Seidenglanz et al., 2012). Therefore, the approximately 200-yr climatic signal revealed in our record is likely associated with solar output, which may indicate that solar forcing is an important control on monsoon intensity.

To clarify the relationship between solar activity and ASM intensity, we compared the LSG δ^{18}O record between 10.2 and 9.1 ka BP and its trend to the sunspot record, a proxy for solar activity (Stuiver et al., 1998; Fig. 5). When the sun is active, fewer cosmic rays reach the earth and, with fewer low clouds, more solar radiation can reach the surface layers below the clouds (e.g., Svensmark and Friis-Christensen, 1997; Svensmark et al., 2017). Visually, the larger amplitude fluctuations in the ASM broadly agree with sunspot events on centennial timescales between 10.2 and 9.1 ka BP (Fig. 5). If the dating errors (Table 1) are taken into account, five centennial-scale strong ASM events roughly correspond to five relatively low solar insolation periods (labeled as vertical grey bars in Fig. 5).

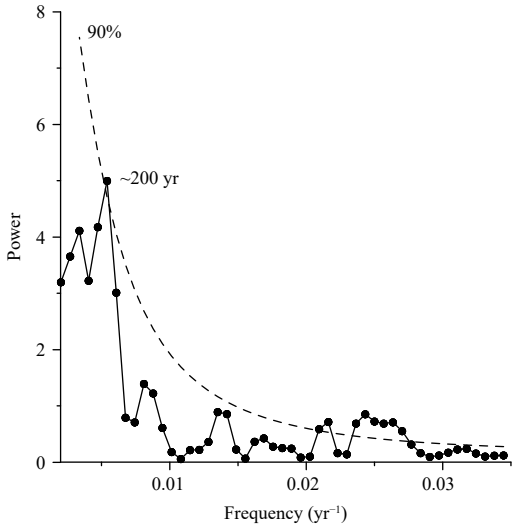

Fig. 4. Power spectrum analysis of the LSG δ^{18}O between 10.2 and 9.1 ka BP. The dashed line indicates the 90% confidence level.

4.2 *Relationship between ENSO and centennial-scale ASM oscillations*

As suggested by previous studies, prior to 8 ka BP, when ice sheets and glaciers were still widespread (Smith et al., 2011), the early Holocene ASM intensity was controlled on centennial and even on decadal timescales by glacial boundary forcing (Fleitmann et al., 2003). The correlations between the ASM variability and the North Atlantic circulation have been widely discussed on multiple timescales (e.g., Fleitmann et al., 2003; Wang et al., 2005). The dominance of the 200-yr cycle in our record between 10.2 and 9.1 ka BP is quite apparent in the time spectra (Fig. 4). Therefore, we focus on the 200-yr cycle in the fluctuations of the ASM and its relationship with ENSO variability during this interval. The LSG δ^{18}O record appears to agree well with the simulated paleo-ENSO record (Liu et al., 2014) available for the early Holocene (Fig. 6), especially for the variations in the frequency. The simulated ENSO data (Fig. 6) are from a model that used the complete set of realistic climate forces: orbital, greenhouse gases, continental ice sheets, and melt water discharge (Liu et al., 2014). These paleo-ENSO data have been extensively used to discuss the close relationship between ENSO and regional climate changes on the centennial (Ning et al., 2017) and submillennial (Zhu et al., 2017) timescales. The cross-wavelet analyses between our δ^{18}O record and the ENSO variance show a strong 200-yr cycle, which is related to the Suess or de Vries cycle of solar activity during the early Holocene.

Our observed ASM–ENSO relationship (Fig. 6) is opposite to that from previous findings. Based on a stalagmite δ^{18}O record from Southeast China for the past 200 years, Zhang et al. (2018) suggested that less summer monsoon precipitation and/or more non-summer monsoon precipitation was associated with El Niño events on interannual to interdecadal timescales. In tree ring re-

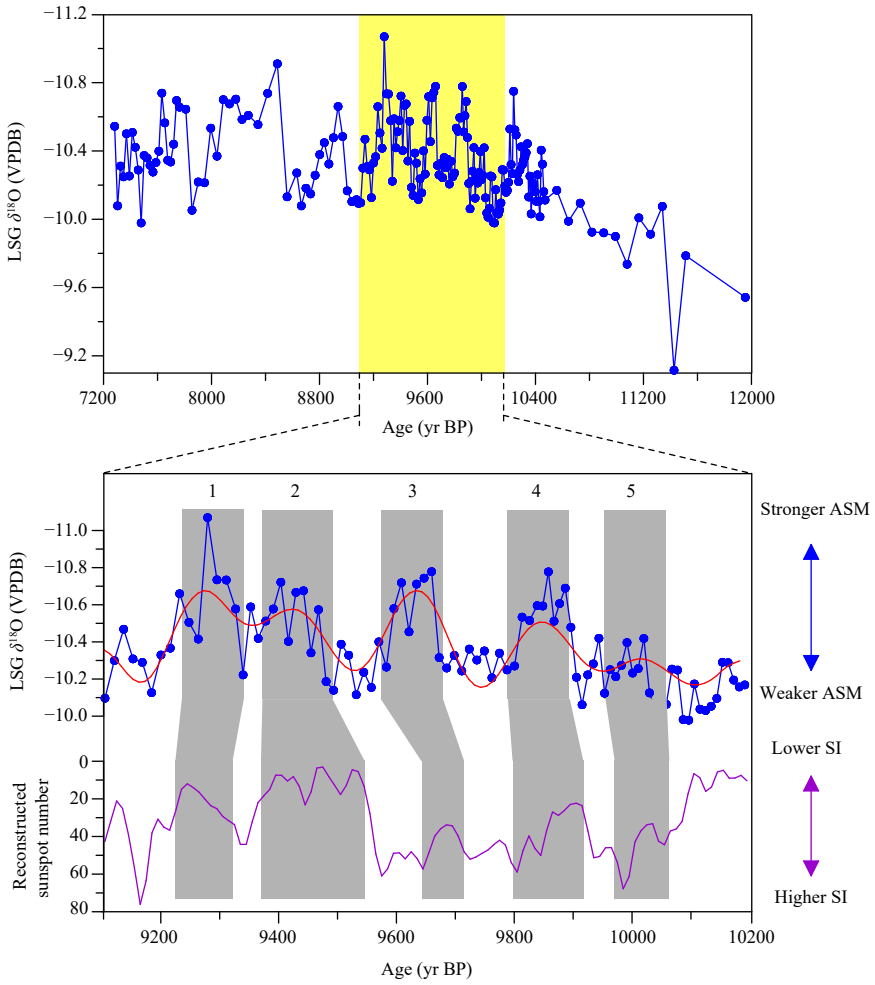

Fig. 5. Correlation of the centennial-scale cycles of the LSG δ^{18}O and the reconstructed sunspot number between 10.2 and 9.1 ka BP. The upper panel shows the LSG δ^{18}O record during the early Holocene with a yellow bar indicating the interval between 10.2 and 9.1 ka BP (blue; this study). The LSG δ^{18}O record between 10.2 and 9.1 ka BP (blue) and its centennial trend (red) are shown in an enlarged window in the lower panel, with the reconstructed sunspot number record (purple; Stuiver et al., 1998). The vertical grey bars indicate five strong Asian summer monsoon stages, which roughly correspond to five relatively low solar insolation (SI) periods.

cords, four historical Asian droughts during the last millennium were all linked to El Niño (Cook et al., 2010). Stalagmite studies in central China have suggested that more positive δ^{18}O (weak monsoon) is related to El Niño on the millennial scale during the past three millennia (Zhao et al., 2016). During the early Holocene, the same ASM–ENSO relationship as that from the above studies was found by using proxy and simulated data on the millennial scale (Marchitto et al., 2010; Jin et al., 2014). A typical mechanism is responsible for the inverse relationship between the ASM and ENSO from modern observations (e.g., Rasmusson and Carpenter, 1983; Ropelewski and Halpert, 1987; Webster and Yang, 1992). During a warm ENSO event with anomalously high SSTs over the eastern tropical Pacific, the convection in the western Pacific shifts to the central and eastern Pacific, which then suppresses the convection in the Asian monsoon region and the western Pacific warm pool region, thus resulting in monsoon failure (e.g., Lau and Nath, 2000; Wang et al., 2003). Due to the dating uncertainty of about 100 yr during our focused interval, the ASM–ENSO relationship in Fig. 6 would change to a different phasing. A 180° phase change would follow most of the studies mentioned above, but would require a systematic shift of about 100 yr. This approximately 100-yr shift is likely, but needs the upper limit of our chronology.

The relationship between ENSO and regional precipitation is spatially heterogeneous (Zhang et al., 2016), which could be applied to explain the relationship shown in Fig. 6. The Yangtze River valley, where Loushanguan Cave is located, is a region where a strong (weak) ASM state corresponds to a warm (cold) ENSO. Huang and Wu (1989), using data from 1950 to 1980, found that a warm ENSO event coincides with droughts in southern

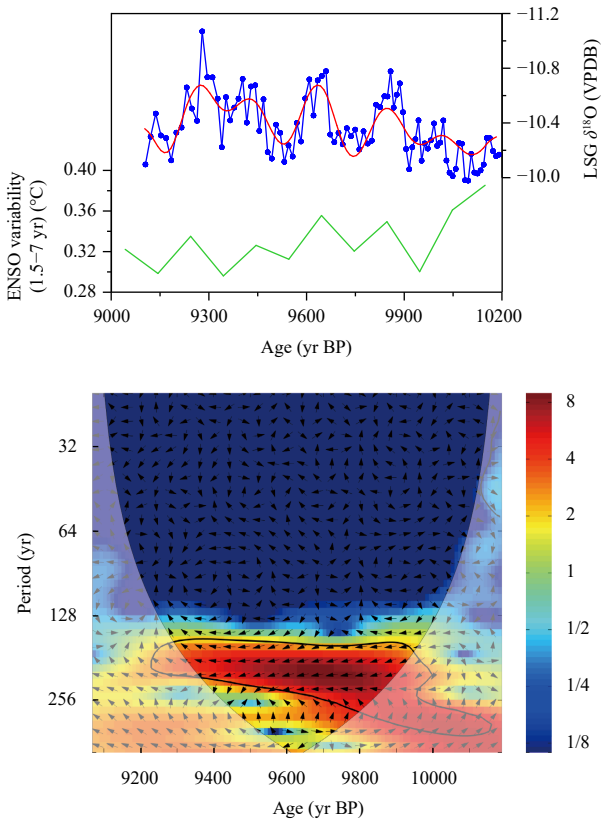

Fig. 6. Correlation of the centennial-scale cycles of the LSG δ^{18}O and ENSO variances between 10.2 and 9.1 ka BP. In the upper panel, the LSG δ^{18}O record between 10.2 and 9.1 ka BP (blue) and its centennial trend (red; this study) are correlated with the simulated ENSO amplitude in a 100-yr window based on observation data [shown as standard deviation of Niño3.4 (a region bounded by 5°S–5°N, 170°–120°W) interannual (1.5–7 yr) sea surface temperature variability] (green; Liu et al., 2014). The cross-wavelet power (shading) between the LSG δ^{18}O and ENSO variances during the interval of 10.2–9.1 ka BP is shown in the lower panel. The thick black contour denotes the 5% significance level against red noise, and the cone of influence (where edge effects might distort the picture) is shown as a lighter shade. Contours are for variance units. The relative phase relationship is shown as black arrows (with in-phase pointing right, anti-phase pointing left, and the ASM leading ENSO by 90° pointing straight down). The black arrows pointing left in the thick black contour mean that the δ^{18}O and ENSO variances are anti-phase on an approximately 200-yr cycle (strong monsoon intervals are related to El Niño-like conditions).

and northern China and floods in central China in the Yangtze River valley and the Huaihe valley. Zhang et al. (2016) established a significant year-round relationship between ENSO and the Yangtze River basin's summer precipitation by combining the Niño3.4 and Niño-A indices, suggesting more precipitation arising from El Niño. This mechanism is discussed in more detail in several papers (e.g., Chang et al., 2000; Wang et al., 2000). During El Niño events, the entire Walker circulation weakens and the locus of rainfall and ascent through the troposphere move eastward (e.g., Ropelewski and Halpert, 1996). At the same time, the subtropical ridge also extends farther to the west from the previous winter to the following fall, resulting in an 850-hPa anomalous anticyclone near the southeast coast of China during the spring and early summer (Chang et al., 2000; Wang et al., 2000). This anticyclone blocks the pre-Meiyu and Meiyu fronts from moving southward, thus causing more summer precipitation over the Yangtze River valley (Chang et al., 2000). During a La Niña event, warmer western Pacific and stronger Philippines convection shift the western Pacific subtropical high northward. Accordingly, the Yangtze River valley tends to experience less rainfall, whereas southern and northern China are characterized by more rainfall (Huang and Sun, 1992).

The significant approximately 200-yr cycle in our record, as revealed by spectral power analyses, points to a pronounced influence of solar activity on the ASM climate on the centennial scale. Here, ENSO may plausibly have acted as a mediator between the sun and the monsoon climate. If there is heating (cooling) over the entire tropics, then the Pacific will warm (cool) more in the west than in the east because the imposed forcing is almost equally balanced by the change in the heat flux and the vertical advection of temperature in the eastern equatorial ocean. The dynamical feedback that makes it harder for the SST to change in the east has earned the name "the thermostat mechanism" (Clement et al., 1996). The air/sea feedbacks [the Bjerknes (1969) feedback] will amplify solar forces to produce persistent, El Niño-like (La Niña-like), SST anomalies at times of decreased irradiance (increased irradiance) (Emile-Geay et al., 2007). The ASM–ENSO relationship observed here is a more direct analogue to the observed modern interannual variability, which may have great potential to predict future ASM changes.

5. Summary

Based on ^{230}Th dates and oxygen isotope data, we present an ASM history for the early Holocene. Our record shows similar variations to other cave records in the ASM region that generally follow the boreal insolation. There are clear centennial fluctuations between 10.2 and 9.1 ka BP, with an approximately 11-yr resolution, and more accurate dates than during other intervals. A significant approximately 200-yr cycle between 10.2 and 9.1 ka BP, as revealed by the spectral power analyses, was globally significant and was probably forced by the Suess or de Vries cycle of solar activity. A strong coherence between the ASM and ENSO was observed via the

cross-wavelet analyses at this cycle. The relationship between a strong (weak) ASM state and a warm (cold) ENSO is consistent with modern meteorological observations but contrasts with previous studies on regions far from the Meiyu belt. We argue that the centennial fluctuations of the ASM are a fundamental characteristic forced by the solar activity, with the ENSO variability as a mediator. The relationship between ENSO and the ASM was spatially heterogeneous on the centennial scale during the early Holocene, which is a more direct analogue to the observed modern interannual variability.

Acknowledgments. We are grateful to the Editor and two anonymous reviewers for their constructive feedbacks that helped improve the manuscript. We would also like to thank Dr. Zhengyao Lu at Lund University for help with describing the simulated ENSO data and Dr. Qingfeng Shao at Nanjing Normal University for help with the U–Th dating.

REFERENCES

Anderson, R. Y., 1992: Possible connection between surface winds, solar activity and the Earth's magnetic field. *Nature*, **358**, 51–53, doi: 10.1038/358051a0.

Berger, A. L., 1978: Long-term variations of caloric insolation resulting from the Earth's orbital elements. *Quat. Res.*, **9**, 139–167, doi: 10.1016/0033-5894(78)90064-9.

Bjerknes, J., 1969: Atmospheric teleconnections from the equatorial Pacific. *Mon. Wea. Rev.*, **97**, 163–172, doi: 10.1175/1520-0493(1969)097<0163:ATFTEP>2.3.CO;2.

Burns, S. J., D. Fleitmann, M. Mudelsee, et al., 2002: A 780-year annually resolved record of Indian Ocean monsoon precipitation from a speleothem from south Oman. *J. Geophys. Res. Atmos.*, **107**, ACL 9-1–ACL 9-9, doi: 10.1029/2001JD001281.

Cai, Y. J., H. W. Zhang, H. Cheng, et al., 2012: The Holocene Indian monsoon variability over the southern Tibetan Plateau and its teleconnections. *Earth Planet. Sci. Lett.*, **335–336**, 135–144, doi: 10.1016/j.epsl.2012.04.035.

Carré, M., J. P. Sachs, S. Purca, et al., 2014: Holocene history of ENSO variance and asymmetry in the eastern tropical Pacific. *Science*, **345**, 1045–1048, doi: 10.1126/science.1252220.

Chang, C.-P., Y. S. Zhang, and T. Li, 2000: Interannual and interdecadal variations of the East Asian summer monsoon and tropical Pacific SSTs. Part I: Roles of the subtropical ridge. *J. Climate*, **13**, 4310–4325, doi: 10.1175/1520-0442(2000)013<4310:IAIVOT>2.0.CO;2.

Chen, L. X., M. Dong, and Y. N. Shao, 1992: The characteristics of interannual variations on the East Asian monsoon. *J. Meteor. Soc. Japan*, **70**, 397–421, doi: 10.2151/jmsj1965.70.1b_397.

Chen, S., S. S. Hoffmann, D. C. Lund, et al., 2016: A high-resolution speleothem record of western equatorial Pacific rainfall: Implications for Holocene ENSO evolution. *Earth Planet. Sci. Lett.*, **442**, 61–71, doi: 10.1016/j.epsl.2016.02.050.

Cheng, H., R. L. Edwards, J. Hoff, et al., 2000: The half-lives of uranium-234 and thorium-230. *Chem. Geol.*, **169**, 17–33, doi: 10.1016/S0009-2541(99)00157-6.

Cheng, H., R. L. Edwards, W. S. Broecker, et al., 2009: Ice age terminations. *Science*, **326**, 248–252, doi: 10.1126/science.1177840.

Cheng, H., R. L. Edwards, C.-C. Shen, et al., 2013: Improvements in ^{230}Th dating, ^{230}Th and ^{234}U half-life values, and U–Th isotopic measurements by multi-collector inductively coupled plasma mass spectrometry. *Earth Planet. Sci. Lett.*, **371–372**, 82–91, doi: 10.1016/j.epsl.2013.04.006.

Clement, A. C., R. Seager, M. A. Cane, et al., 1996: An ocean dynamical thermostat. *J. Climate*, **9**, 2190–2196, doi: 10.1175/1520-0442(1996)009<2190:AODT>2.0.CO;2.

Collins, M., S. An, W. J. Cai, et al., 2010: The impact of global warming on the tropical Pacific Ocean and El Niño. *Nat. Geosci.*, **3**, 391–397, doi: 10.1038/ngeo868.

Cook, E. R., B. M. Buckley, and R. D. D'Arrigo, 1996: Interdecadal climate oscillations in the Tasmanian sector of the Southern Hemisphere: Evidence from tree rings over the past three millennia. *Climatic Variations and Forcing Mechanisms of the Last 2000 Years*, Jones, P. D., R. S. Bradley, and J. Jouzel, Eds., Springer, Berlin, 141–160, doi: 10.1007/978-3-642-61113-1_8.

Cook, E. R., K. J. Anchukaitis, B. M. Buckley, et al., 2010: Asian monsoon failure and megadrought during the last millennium. *Science*, **328**, 486–489, doi: 10.1126/science.1185188.

Corbett, L. B., N. E. Young, P. R. Bierman, et al., 2011: Paired bedrock and boulder ^{10}Be concentrations resulting from early Holocene ice retreat near Jakobshavn Isfjord, western Greenland. *Quat. Sci. Rev.*, **30**, 1739–1749, doi: 10.1016/j.quascirev.2011.04.001.

Ding, Y. H., 2004: Seasonal march of the East Asian summer monsoon. *East Asian Monsoon*, Chang, C.-P., Ed., World Scientific Press, New Jersey, 3–53, doi: 10.1142/9789812701411_0001.

Dong, J. G., Y. J. Wang, H. Cheng, et al., 2010: A high-resolution stalagmite record of the Holocene East Asian monsoon from Mt Shennongjia, central China. *The Holocene*, **20**, 257–264, doi: 10.1177/0959683609350393.

Dorale, J. A., and Z. H. Liu, 2009: Limitations of Hendy Test criteria in judging the paleoclimatic suitability of speleothems and the need for replication. *J. Cave Karst Stud.*, **71**, 73–80.

Dykoski, C. A., R. L. Edwards, H. Cheng, et al., 2005: A high-resolution, absolute-dated Holocene and deglacial Asian monsoon record from Dongge Cave, China. *Earth Planet. Sci. Lett.*, **233**, 71–86, doi: 10.1016/j.epsl.2005.01.036.

Emile-Geay, J., M. Cane, R. Seager, et al., 2007: El Niño as a mediator of the solar influence on climate. *Paleoceanogr. Paleoclimatol.*, **22**, PA3210, doi: 10.1029/2006PA001304.

Fleitmann, D., S. J. Burns, M. Mudelsee, et al., 2003: Holocene forcing of the Indian monsoon recorded in a stalagmite from southern Oman. *Science*, **300**, 1737–1739, doi: 10.1126/science.1083130.

Huang, R. H., and L. Lu, 1989: Numerical simulation of the relationship between the anomaly of subtropical high over East Asia and the convective activities in the western tropical Pacific. *Adv. Atmos. Sci.*, **6**, 202–214, doi: 10.1007/BF02658016.

Huang, R. H., and Y. F. Wu, 1989: The influence of ENSO on the summer climate change in China and its mechanism. *Adv. At-*

mos. Sci., **6**, 21–32, doi: 10.1007/BF02656915.

Huang, R. H., and F. Y. Sun, 1992: Impacts of the tropical western Pacific on the East Asian summer monsoon. *J. Meteor. Soc. Japan*, **70**, 243–256, doi: 10.2151/jmsj1965.70.1b_243.

Huang, W., Y. J. Wang, H. Cheng, et al., 2016: Multi-scale Holocene Asian monsoon variability deduced from a twin-stalagmite record in southwestern China. *Quat. Res.*, **86**, 34–44, doi: 10.1016/j.yqres.2016.05.001.

Hughes, A. L. C., E. Rainsley, T. Murray, et al., 2012: Rapid response of Helheim Glacier, southeast Greenland, to early Holocene climate warming. *Geology*, **40**, 427–430, doi: 10.1130/g32730.1.

Jaffey, A. H., K. F. Flynn, L. E. Glendenin, et al., 1971: Precision measurement of half-lives and specific activities of ^{235}U and ^{238}U. *Phys. Rev. C*, **4**, 1889–1906, doi: 10.1103/physrevc.4.1889.

Jin, L. Y., B. Schneider, W. Park, et al., 2014: The spatial–temporal patterns of Asian summer monsoon precipitation in response to Holocene insolation change: A model-data synthesis. *Quat. Sci. Rev.*, **85**, 47–62, doi: 10.1016/j.quascirev.2013.11.004.

Ju, J. H., and J. Slingo, 1995: The Asian summer monsoon and ENSO. *Quart. J. Roy. Meteor. Soc.*, **121**, 1133–1168, doi: 10.1002/qj.49712152509.

Kinter III, J. L., K. Miyakoda, and S. Yang, 2002: Recent change in the connection from the Asian monsoon to ENSO. *J. Climate*, **15**, 1203–1215, doi: 10.1175/1520-0442(2002)015<1203:RCITCF>2.0.CO;2.

Kumar, K. K., B. Rajagopalan, and M. A. Cane, 1999: On the weakening relationship between the Indian monsoon and ENSO. *Science*, **284**, 2156–2159, doi: 10.1126/science.284.5423.2156.

Kumar, K. K., B. Rajagopalan, M. Hoerling, et al., 2006: Unraveling the mystery of Indian monsoon failure during El Niño. *Science*, **314**, 115–119, doi: 10.1126/science.1131152.

Larsen, N. K., K. H. Kjær, J. Olsen, et al., 2011: Restricted impact of Holocene climate variations on the southern Greenland Ice Sheet. *Quat. Sci. Rev.*, **30**, 3171–3180, doi: 10.1016/j.quascirev.2011.07.022.

Lau, K.-M., and H. Y. Weng, 2001: Coherent modes of global SST and summer rainfall over China: An assessment of the regional impacts of the 1997–98 El Niño. *J. Climate*, **14**, 1294–1308, doi: 10.1175/1520-0442(2001)014<1294:CMOGSA>2.0.CO;2.

Lau, N.-C., and M. J. Nath, 2000: Impact of ENSO on the variability of the Asian–Australian monsoons as simulated in GCM experiments. *J. Climate*, **13**, 4287–4309, doi: 10.1175/1520-0442(2000)013<4287:IOEOTV>2.0.CO;2.

Li, J. P., Z. W. Wu, Z. H. Jiang, et al., 2010: Can global warming strengthen the East Asian summer monsoon? *J. Climate*, **23**, 6696–6705, doi: 10.1175/2010JCLI3434.1.

Liu, D. B., Y. J. Wang, H. Cheng, et al., 2015: Cyclic changes of Asian monsoon intensity during the early mid-Holocene from annually-laminated stalagmites, central China. *Quat. Sci. Rev.*, **121**, 1–10, doi: 10.1016/j.quascirev.2015.05.003.

Liu, Z. Y., Z. Y. Lu, X. Y. Wen, et al., 2014: Evolution and forcing mechanisms of El Niño over the past 21,000 years. *Nature*, **515**, 550–553, doi: 10.1038/nature13963.

Marchitto, T. M., R. Muscheler, J. D. Ortiz, et al., 2010: Dynamical response of the tropical Pacific Ocean to solar forcing during the early Holocene. *Science*, **330**, 1378–1381, doi: 10.1126/science.1194887.

Moy, C. M., G. O. Seltzer, D. T. Rodbell, et al., 2002: Variability of El Niño/Southern Oscillation activity at millennial timescales during the Holocene epoch. *Nature*, **420**, 162–165, doi: 10.1038/nature01194.

Muñoz, A., M. Bartolomé, A. Muñoz, et al., 2015: Solar influence and hydrological variability during the Holocene from a speleothem annual record (Molinos Cave, NE Spain). *Terra Nova*, **27**, 300–311, doi: 10.1111/ter.12160.

Ning, D. L., E. L. Zhang, W. W. Sun, et al., 2017: Holocene Indian Summer Monsoon variation inferred from geochemical and grain size records from Lake Ximenglongtan, southwestern China. *Palaeogeogr., Palaeoclimatol., Palaeoecol.*, **487**, 260–269, doi: 10.1016/j.palaeo.2017.09.008.

Ninomiya, K., 2004: Large- and mesoscale features of Meiyu-Baiu front associated with intense rainfalls. *East Asian Monsoon*, Chang, C.-P., Ed., World Scientific Press, New Jersey, 404–435, doi: 10.1142/9789812701411_0011.

Nitta, T., and Z.-Z. Hu, 1996: Summer climate variability in China and its association with 500 hPa height and tropical convection. *J. Meteor. Soc. Japan*, **74**, 425–445, doi: 10.2151/jmsj1965.74.4_425.

Pai, D. S., 2004: A possible mechanism for the weakening of El Niño-monsoon relationship during the recent decade. *Meteor. Atmos. Phys.*, **86**, 143–157, doi: 10.1007/s00703-003-0608-8.

Parthasarathy, B., A. A. Munot, and D. R. Kothawale, 1994: All-India monthly and seasonal rainfall series: 1871–1993. *Theor. Appl. Climatol.*, **49**, 217–224, doi: 10.1007/BF00867461.

Peterson, L. C., J. T. Overpeck, N. G. Kipp, et al., 1991: A high-resolution Late Quaternary upwelling record from the anoxic Cariaco Basin, Venezuela. *Paleoceanogr. Paleoclimatol.*, **6**, 99–119, doi: 10.1029/90PA02497.

Rasmusson, E. M., and T. H. Carpenter, 1983: The relationship between eastern equatorial Pacific sea surface temperatures and rainfall over India and Sri Lanka. *Mon. Wea. Rev.*, **111**, 517–528, doi: 10.1175/1520-0493(1983)111<0517:TRBEEP>2.0.CO;2.

Raspopov, O. M., V. A. Dergachev, J. Esper, et al., 2008: The influence of the de Vries (~200-year) solar cycle on climate variations: Results from the central Asian mountains and their global link. *Palaeogeogr., Palaeoclimatol., Palaeoecol.*, **259**, 6–16, doi: 10.1016/j.palaeo.2006.12.017.

Rodó, X., and M.-A. Rodriguez-Arias, 2004: El Niño–Southern Oscillation: Absent in the early Holocene? *J. Climate*, **17**, 423–426, doi: 10.1175/1520-0442(2004)017<0423:ENOAIT>2.0.CO;2.

Ropelewski, C. F., and M. S. Halpert, 1987: Global and regional scale precipitation patterns associated with the El Niño/Southern Oscillation. *Mon. Wea. Rev.*, **115**, 1606–1626, doi: 10.1175/1520-0493(1987)115<1606:GARSPP>2.0.CO;2.

Ropelewski, C. F., and M. S. Halpert, 1996: Quantifying Southern Oscillation–precipitation relationships. *J. Climate*, **9**, 1043–1059,doi:10.1175/1520-0442(1996)009<1043:QSOPR>2.0.CO;2.

Seidenglanz, A., M. Prange, V. Varma, et al., 2012: Ocean temperature response to idealized Gleissberg and de Vries solar cycles in a comprehensive climate model. *Geophys. Res. Lett.*, **39**, L22602, doi: 10.1029/2012GL053624.

Shen, S., and K.-M. Lau, 1995: Biennial oscillation associated with the East Asian summer monsoon and tropical sea surface temperatures. *J. Meteor. Soc. Japan*, **73**, 105–124, doi: 10.2151/jmsj1965.73.1_105.

Smith, D. E., S. Harrison, C. R. Firth, et al., 2011: The early Holocene sea level rise. *Quat. Sci. Rev.*, **30**, 1846–1860, doi: 10.1016/j.quascirev.2011.04.019.

Springer, G. S., H. D. Rowe, B. Hardt, et al., 2008: Solar forcing of Holocene droughts in a stalagmite record from West Virginia in east-central North America. *Geophys. Res. Lett.*, **35**, L17703, doi: 10.1029/2008GL034971.

Stuiver, M., P. J. Reimer, E. Bard, et al., 1998: INTCAL98 radiocarbon age calibration, 24,000–0 cal BP. *Radiocarbon*, **40**, 1041–1083, doi: 10.1017/S0033822200019123.

Svensmark, H., and E. Friis-Christensen, 1997: Variation of cosmic ray flux and global cloud coverage—a missing link in solar–climate relationships. *J. Atmos. Solar-Terr. Phys.*, **59**, 1225–1232, doi: 10.1016/S1364-6826(97)00001-1.

Svensmark, H., M. B. Enghoff, N. J. Shaviv, et al., 2017: Increased ionization supports growth of aerosols into cloud condensation nuclei. *Nat. Commun.*, **8**, 2199, doi: 10.1038/s41467-017-02082-2.

Wang, B., R. G. Wu, and X. H. Fu, 2000: Pacific–East Asian teleconnection: How does ENSO affect East Asian climate? *J. Climate*, **13**, 1517–1536, doi: 10.1175/1520-0442(2000)013<1517:PEATHD>2.0.CO;2.

Wang, B., R. G. Wu, and T. Li, 2003: Atmosphere–warm ocean interaction and its impacts on Asian–Australian monsoon variation. *J. Climate*, **16**, 1195–1211, doi: 10.1175/1520-0442(2003)16<1195:AOIAII>2.0.CO;2.

Wang, B., Z. W. Wu, J. P. Li, et al., 2008: How to measure the strength of the East Asian summer monsoon. *J. Climate*, **21**, 4449–4463, doi: 10.1175/2008JCLI2183.1.

Wang, B., F. Huang, Z. W. Wu, et al., 2009: Multi-scale climate variability of the South China Sea monsoon: A review. *Dyn. Atmos. Oceans*, **47**, 15–37, doi: 10.1016/j.dynatmoce.2008.09.004.

Wang, H. J., 2002: The instability of the East Asian summer monsoon–ENSO relations. *Adv. Atmos. Sci.*, **19**, 1–11, doi: 10.1007/s00376-002-0029-5.

Wang, Y. J., H. Cheng, R. L. Edwards, et al., 2005: The Holocene Asian monsoon: Links to solar changes and North Atlantic climate. *Science*, **308**, 854–857, doi: 10.1126/science.1106296.

Webster, P. J., and S. Yang, 1992: Monsoon and ENSO: Selectively interactive systems. *Quart. J. Roy. Meteor. Soc.*, **118**, 877–926, doi: 10.1002/qj.49711850705.

Wu, D., X. M. Chen, F. Y. Lyu, et al., 2018: Decoupled early Holocene summer temperature and monsoon precipitation in southwest China. *Quat. Sci. Rev.*, **193**, 54–67, doi: 10.1016/j.quascirev.2018.05.038.

Wu, Z. W., J. P. Li, Z. H. Jiang, et al., 2012: Possible effects of the North Atlantic Oscillation on the strengthening relationship between the East Asian summer monsoon and ENSO. *Int. J. Climatol.*, **32**, 794–800, doi: 10.1002/joc.2309.

Zhang, H. W., H. Cheng, C. Spötl, et al., 2018: A 200-year annually laminated stalagmite record of precipitation seasonality in southeastern China and its linkages to ENSO and PDO. *Sci. Rep.*, **8**, 12344, doi: 10.1038/s41598-018-30112-6.

Zhang, W. J., F.-F. Jin, M. F. Stuecker, et al., 2016: Unraveling El Niño's impact on the East Asian monsoon and Yangtze River summer flooding. *Geophys. Res. Lett.*, **43**, 11375–11382, doi: 10.1002/2016GL071190.

Zhao, K., Y. J. Wang, R. L. Edwards, et al., 2015: A high-resolved record of the Asian summer monsoon from Dongge Cave, China for the past 1200 years. *Quat. Sci. Rev.*, **122**, 250–257, doi: 10.1016/j.quascirev.2015.05.030.

Zhao, K., Y. J. Wang, R. L. Edwards, et al., 2016: Contribution of ENSO variability to the East Asian summer monsoon in the late Holocene. *Palaeogeogr., Palaeoclimatol., Palaeoecol.*, **449**, 510–519, doi: 10.1016/j.palaeo.2016.02.044.

Zhao, X. H., and X. S. Feng, 2015: Correlation between solar activity and the local temperature of Antarctica during the past 11,000 years. *J. Atmos. Solar-Terr. Phys.*, **122**, 26–33, doi: 10.1016/j.jastp.2014.11.004.

Zhu, Z. M., J. M. Feinberg, S. C. Xie, et al., 2017: Holocene ENSO-related cyclic storms recorded by magnetic minerals in speleothems of central China. *Proc. Natl. Acad. Sci. USA*, **114**, 852–857, doi: 10.1073/pnas.1610930114.

Tech & Copy Editor: Qi WANG